applied sciences

MDPI

Article

The Investigation of the Fracture Behavior of a Chinese 9% Cr Steel Welded Joint under Creep-Fatigue Interactive Loading

Yuebing Li [1,2], Yuxuan Song [2,*], Pan Liu [1] and Ting Jin [1]

[1] State Key Laboratory of Nuclear Power Safety Monitoring Technology and Equipment, China Nuclear Power Engineering Co., Ltd., Building 5#, Tianan Cyber Park, Shenzhen 518172, China; ybli@zjut.edu.cn (Y.L.); liup@cgnpc.com.cn (P.L.); jinting@cgnpc.com.cn (T.J.)

[2] Institute of Process Equipment and Control Engineering, Zhejiang University of Technology, Liuhe Road 288#, Xihu Zone, Hangzhou 310032, China

* Correspondence: songyux@zjut.edu.cn

Abstract: To understand the premature-fracture mechanisms of long-term service damage of an advanced alloy's (Chinese P92 steel) welded joint, the creep-fatigue (CF) experiments with holding times of 30, 120, 300, 600 and 900 s were individually performed at 923 K. The cyclic softening, inelastic-strain amplitudes and stress-relaxation behaviors were compared between welded and base-metal (BM) specimens. From the results, the failure stage of the welded specimens occupies 45% of the lifetime fraction, while it only takes up 20% of the lifetime fraction in BM specimens with short holding times (30 and 120 s). Furthermore, only two softening stages were observed for both kinds of CF specimens with long holding times. The absence of a third softening stage in longer-held specimens indicates that the processes of macroscopic-crack initiation, propagation and rupture were accelerated. Based on the observation of the fracture surfaces, the fracture mechanism shifted from fatigue-dominated damage to creep-fatigue interaction when the holding period was increased.

Keywords: P92 steel; welded joint; creep-fatigue interaction; fracture

check for updates

Citation: Li, Y.; Song, Y.; Liu, P.; Jin, T. The Investigation of the Fracture Behavior of a Chinese 9% Cr Steel Welded Joint under Creep-Fatigue Interactive Loading. *Appl. Sci.* **2021**, *11*, 9983. https://doi.org/10.3390/app11219983

Academic Editor: Xijia Wu

Received: 3 October 2021
Accepted: 21 October 2021
Published: 25 October 2021

Publisher's Note: MDPI stays neutral with regard to jurisdictional claims in published maps and institutional affiliations.

Copyright: © 2021 by the authors. Licensee MDPI, Basel, Switzerland. This article is an open access article distributed under the terms and conditions of the Creative Commons Attribution (CC BY) license (https://creativecommons.org/licenses/by/4.0/).

1. Introduction

Due to the attempt to reduce carbon dioxide emissions, fossil fuel and nuclear power plants will be operating at higher temperatures, leading to an increase in the requirement of material properties and structural-integrity assessments. The next generation of ultra-supercritical units (USC) will be improved to over 873 K, and even up to 973 K for advanced fossil-power plants. At such high temperatures, USC units are frequently subjected to creep-fatigue (CF) loading by repeated start-up and shut-down cycles. Creep-fatigue interaction is reported to be more detrimental to the high-temperature components in comparison to creep or fatigue damage [1–3]. Hence, an understanding of the CF behavior of P92 steel at elevated temperatures has increased the concerns of researchers and engineers. Gopinath et al. [4] observed the microstructural evolution of P92 steel during CF testing and examined the damage mechanisms at the micro scale. Zhang et al. [5,6] studied the remnant tensile strength and creep resistance of 9% Cr steel after prior CF loading and concluded that the reduction in the remnant creep property was resulted from the growth of martensitic laths. To increase the operating temperature of units, the microstructural evolution and reduced-material properties at higher temperatures should be urgently studied. Therefore, it is necessary to investigate the creep-fatigue interactive mechanism of in-service alloys at over 873 K.

Although advanced alloys like 9% Cr steel have been extensively utilized in power units due to their excellent creep resistances, their welded joints are regarded as being weak regions that could be the sources of creep-fatigue failure during service. Based on the results of fatigue tests, Veerababu et al. [7] found the fatigue strength of P92 steel welded joints to be significantly degraded by comparing it to the fatigue strength of

the homogeneous base metal. Pandey et al. [8] studied the formation mechanism of various microstructures in different regions of a P92 steel welded joint and found that the welding process produced a heterogeneous microstructure in the heat-affected zone (HAZ) of the welded joint. Those regions have different sensitivities to the macroscopical CF loading [9–12]. Relying on nanoindentation, Gao et al. [13] investigated the remnant creep behavior of the base metal (BM), fine-grain heat-affected zone (FGHAZ), coarse-grain heat-affected zone (CGHAZ) and weld metal (WM) for a CF-tested P92-welded joint, and they found remarkable degradations in the creep resistances of the BM and FGHAZ regions. Furthermore, the nucleation and propagation of creep voids are more likely to occur in the FGHAZ [14–16], which was defined as the main reason for the premature failure of the welded joint. On the other hand, creep and fatigue are two competitive factors, which can result in the fatigue-dominated fracture mechanism rather than the creep-fatigue damage mechanism. When the factors of creep-fatigue loading such as holding time, strain rate, strain amplitude and holding mode are changed, the dominant fracture mechanism and the ruptured position in the welded joint are varied. The complexity of creep-fatigue loading and the inhomogeneity of welded joints cooperatively impede the development of the life-prediction method for CF-tested welds.

The life-prediction methods for fatigue fracture and creep-fatigue fracture are totally different [17]. Based on the linear damage rules, the nonlinear damage curve and two-stage linearization approaches, the life-curve modification methods, the approaches based on crack-growth concepts, the continuum-damage mechanics models and energy-based theories, the fatigue life-prediction methods have been widely used for metals and their alloys [18]. As for the life prediction of creep-fatigue fracture, Zhao and Wang have each proposed a modified strain energy density exhaustion model for creep-fatigue life prediction, which can accurately predict the cyclic life of CF-tested high-Cr steels [19,20]. However, if the fatigue life-prediction method is selected to predict the cyclic life of the creep-fatigue-ruptured welds, the accuracy of life prediction can be significantly reduced. Therefore, it is important to study the transformation of the fracture mechanism under different creep-fatigue loadings, so as to provide the experimental data support to the investigation into creep-fatigue life-prediction methods for welds.

This paper focuses on the fracture mechanism of Chinese P92 steel welded joint under CF loading. The strain-controlled CF experiments with holding times of 30, 120, 300, 600 and 900 s were individually performed on welded specimens at 923 K, as well as on base-metal (BM) specimens. The cyclic softening, inelastic strain amplitudes and stress relaxation behaviors are compared between welded and BM specimens. Based on the observation of fracture surfaces, the effects of the holding period on the transformation of fracture mechanisms of welded joints under creep-fatigue loading were systematically studied.

2. Materials and Experimental Procedures

2.1. Materials

A commercial Chinese P92 steel was prepared in this work. Two P92 pipes with thickness, radius and length dimensions of 80 × 840 × 300 mm, respectively, were welded together using submerged arc welding (SAW) and gas tungsten arc welding (GTAW). The morphology of the welded joint is shown in Figure 1a. The welded pipe was then annealed at 1033 K for 2 h followed by air cooling. Finally, a nondestructive inspection was performed in order to confirm that the welded joint met the industrial requirement. The typical chemical composition ranges for P92 steel and wire, along with the specific compositions of the alloy, are listed in Table 1; these compositions meet the requirement of the ASME Boiler & Pressure Vessel Code Part II -2015 [21]. The welded joint was polished and etched using a mixture comprised of 92 mL water, 4 mL hydrofluoric acid and 4 mL nitric acid. The etched microstructures of the BM, FGHAZ, CGHAZ and WM were examined, as shown in Figure 2a–d, respectively. Tempered martensitic laths were observed in the prior austenitic grains. Fine prior austenitic grains were also observed in

the BM and FGHAZ regions, while coarser prior austenitic grains were seen in the CGHAZ and WM regions.

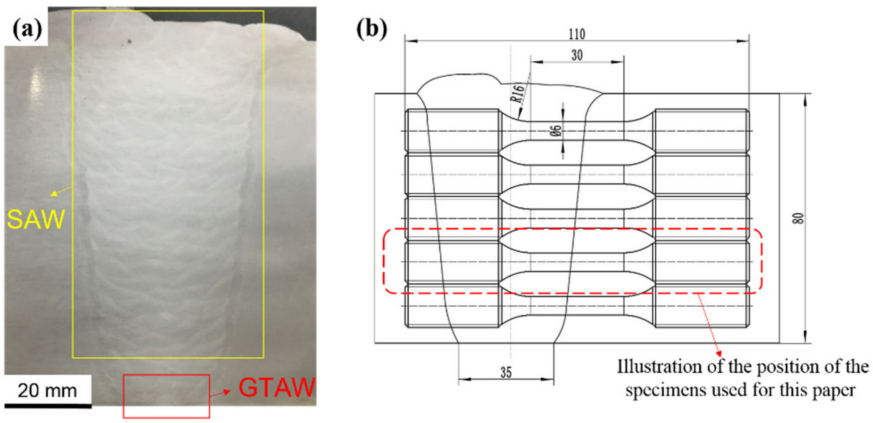

Figure 1. (**a**) Optical macrograph of the welded joint and (**b**) the illustration of the position and geometry of CF specimens from the P92 steel welded joint [22].

Table 1. Chemical compositions of Chinese P92 steel and welded joint (wt.%).

Element	C	Si	Mn	Ni	Cr	Mo	P	S	N	W
P92	0.11	0.245	0.361	0.108	9.220	0.374	0.017	0.008	0.061	1.61
wire	0.095	0.150	0.610	0.680	8.360	0.940	0.011	0.007	0.041	1.58

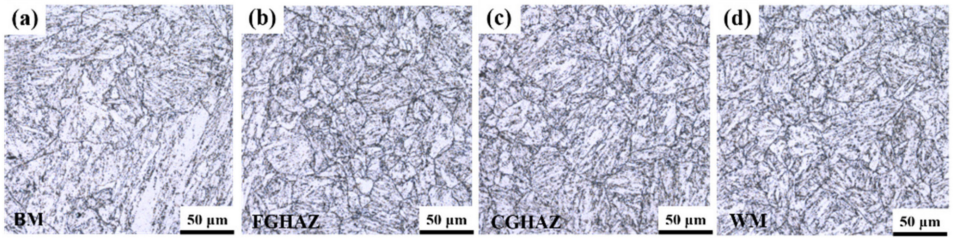

Figure 2. Microstructures in the (**a**) BM, (**b**) FGHAZ, (**c**) CGHAZ and (**d**) WM regions for P92 steel welded joint [22].

2.2. Creep-Fatigue Experiment

To ensure that the initial mechanical properties were similar, the welded specimens in this work were cut from the same position in relation to the welded joint, as shown in Figure 1b. The experiments with all of the as-welded specimens, as well as the base-metal specimens, were conducted in the electronic creep-fatigue testing machine (RPL 100) at 923 K. The trapezoidal wave was employed in the strain-controlled CF experiments, in which there was a constant strain amplitude of 0.2% and a strain rate of 0.001 s^{-1}, as shown in Figure 3. The holding times of 0, 30, 120, 300, 600 and 900 s were used in the CF tests for all of the as-welded and base-metal specimens. The instantaneous gauge length of the specimen was measured by an extensometer (Epsilon, the initial gauge length is 25 mm) during CF tests, for which the data-acquisition frequency was set to 10 Hz. To ensure a uniform temperature in CF specimens, all of the specimens were held for half an hour at 923 K before the test was started. During the testing, the temperature variation was strictly kept at less than 1 K by three S-type thermocouples, which were fixed to the top, middle and bottom of each specimen.

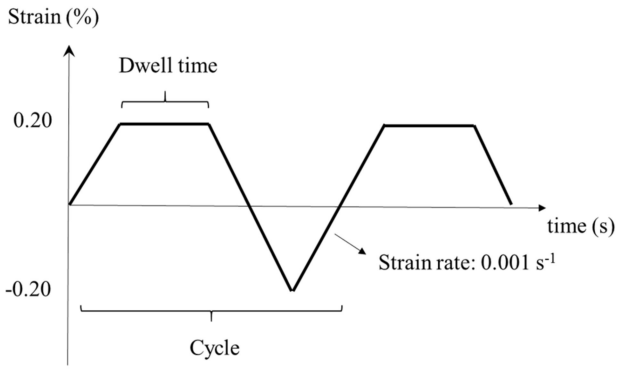

Figure 3. Schematic representation of creep-fatigue test.

3. Results and Discussion

3.1. Cyclic Softening Behavior

Figure 4 exhibits the cyclic life of CF specimens (P92 steel and welded joint) with different holding times. All of the CF specimens were ruptured in the BM regions. Furthermore, the distance of the main crack from the fusion line decreased from 7.2 mm to 1.7 mm for the welded specimens as holding time increased. These results show that the cyclic life of P92 steel decreases as holding time increases. This trend was also observed for welded-joint specimens, except for the specimens with a holding time of 30 s. Compared with the cyclic life of P92 steel, the premature failure only occurred in the welded specimens with holding times of 30 s and 900 s. This observation is different from the reported phenomenon that creep-fatigue interaction can result in the welded joints of 9% Cr steel prematurely fracturing [5,6]. The differing definitions of cyclic life could be the reason for this observation. The previous studies [5,6] proposed the definition of cyclic life, which was defined as a reduction of 10% of the peak tensile stress of the CF specimen at the secondary softening stage. In order to investigate the fracture mechanism, the behaviors of main-crack propagation should be considered in this work. Therefore, the cyclic life of the CF specimens that were used in this investigation was defined as the cycle at the time of occurrence of the actual fracture. The cyclic damage can be characterized by the measured peak tensile stress per cycle during the CF tests.

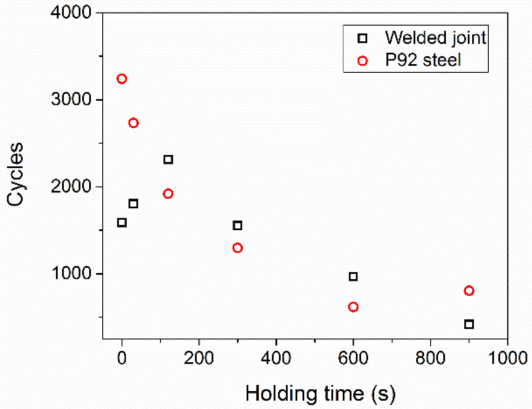

Figure 4. Cyclic life of CF specimens (P92 steel and welded joint) with different holding times.

Figure 5 shows the variations in the measured peak tensile stress values during the creep-fatigue test with different holding times for both specimens. Three distinct softening states were observed: the rapidly softening stage, the steadily softening stage and the failure stage. At the rapidly softening stage, the peak tensile stress rapidly decreased from 250 MPa to 170 MPa, indicating that enhanced dislocation annihilation and degenerated dislocation multiplication were simultaneously occurring. Then, the creep-fatigue interactive progress changed to the steadily softening stage, wherein the annihilation and multiplication of

dislocations were gradually in dynamic equilibrium, which led to a slight decrease in peak tensile stress from 170 MPa to 150 MPa. Finally, macroscopic cracks were formed, and the peak tensile stress began to sharply decrease at the failure stage. In this stage, an interesting phenomenon occurred. At short holding times (30 and 120 s), the failure stage of the welded specimens occupied 45% of the lifetime fraction, while it only took up 20% of the lifetime fraction of the BM specimens, as plotted in Figure 5a. After the normalization of cyclic life (N/Nf), Figure 5a shows that the macroscopic cracks were prematurely initiated in the welded specimens with short holding times. Figure 5b shows the peak tensile stress of BM and welded specimens with long holding times (300, 600 and 900 s) during the CF test. It should be noted that only two softening stages were observed for both kinds of CF specimens with long holding times (300, 600 and 900 s). The absence of a third softening stage in long-held specimens indicates that the processes of macroscopic-crack initiation, propagation and rupture are too rapid to be measured through the variation in peak tensile stress per cycle. This observation also suggests that the fracture mechanism could be gradually changed by increasing holding times for both kinds of specimens.

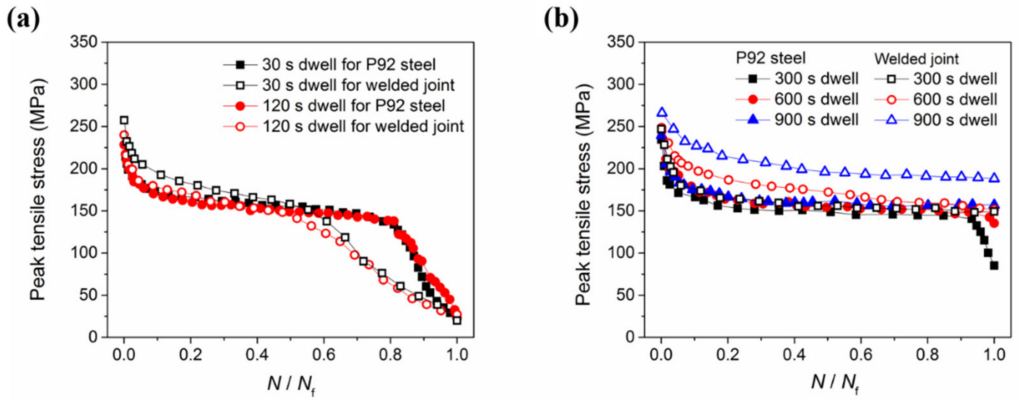

Figure 5. Variations in measured peak tensile stress during the creep-fatigue test with (**a**) short holding times (30 and 120 s) and (**b**) long holding times (300, 600 and 900 s).

On the other hand, the peak tensile stress levels of the welded specimens were enhanced in comparison to the BM specimens with the same holding time, as shown in Figure 5b. The peak tensile stress levels of the welded specimens were observed to increase with increasing holding time, while they remained mostly the same for all of the BM specimens. In the previous study [10], the WM region had a higher value of nanoindentation hardness than the BM and FGHAZ regions. Therefore, the average values of hardness for welded specimens were higher than those of the BM specimens. Since the creep-fatigue experiment is strain-controlled, the peak tensile stress of the welded specimen could be higher than that of the BM specimen at the same strain (0.20%). Furthermore, this change in peak tensile stress level can be related to the discrepancy of inelastic strain between BM and welded specimens. Figure 6 shows the typical strain_stress hysteresis loop of the welded specimen with a holding time of 300 s. It schematically indicates that the inelastic strain amplitude can be directly obtained from the strain-stress hysteresis loop. The creep-fatigue behaviors at the first cycle and the cycle equivalent to 50% of the lifetime fraction are widely reported to be important to the investigation of the damage mechanisms [4,19,20,23]. Figure 7 shows the variations in measured inelastic amplitude during the creep-fatigue test for all of the BM and welded specimens. The inelastic strain amplitude of BM specimens was observed to increase from 0.190% to 0.230% with increasing holding time at the first cycle. Compared with the BM specimens, the enhanced inelastic strain amplitude (0.250% to 0.290%) was estimated for the welded specimens at the first cycle, as shown in Figure 7a. In the previous study [13], the local hardness of the WM and CGHAZ regions were higher than that of the BM and FGHAZ regions before CF testing. Hence, the BM and FGHAZ regions in welded specimens could be subjected to more severe deformation compared with

the BM specimens at the first cycle of the strain-controlled CF tests, resulting in enhanced inelastic strain amplitudes. Figure 7b shows that the inelastic strain amplitude increased to 0.255% (30 s), 0.262% (120 s), 0.270% (300 s), 0.280% (600 s) and 0.292% (900 s) for the BM specimens at 50% of the lifetime fraction. Furthermore, the inelastic strain amplitude of the welded specimens was almost unchanged at 50% of the lifetime fraction, except the one with a 900 s holding time, which slightly decreased to 0.273%. In the previous study [10], the reduction in the hardness of the WM region was more remarkable than in the BM and FGHAZ regions, even though the WM region still had a higher value of hardness due to its high initial hardness. This reduction can be related to the Mo content in the alloy. The chemical composition of the WM zone is dominated by the P92 wire, with a higher Mo content (0.940%) than the P92 steel (0.374%). However, excessive Mo content could reduce the ductility and stability of alloys at high temperatures [24], leading to a remarkable reduction in the hardness of the WM region. The reduction in the hardness of the WM region could gradually induce more deformation to compensate for the local deformation of the FGHAZ and BM regions during the strain-controlled CF test. This process could result in the unchanged inelastic strain amplitudes of welded specimens at macroscopic levels.

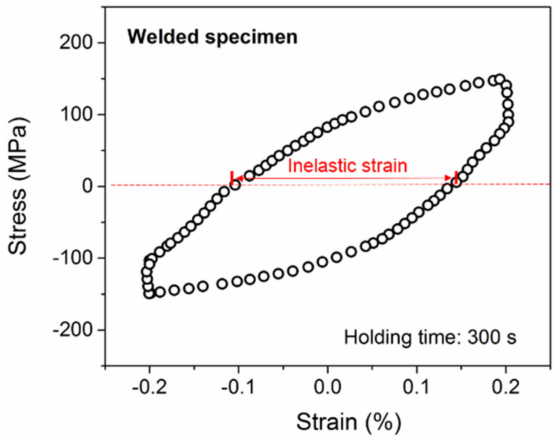

Figure 6. The representative strain-stress hysteresis loop of the welded specimen with a holding time of 300 s.

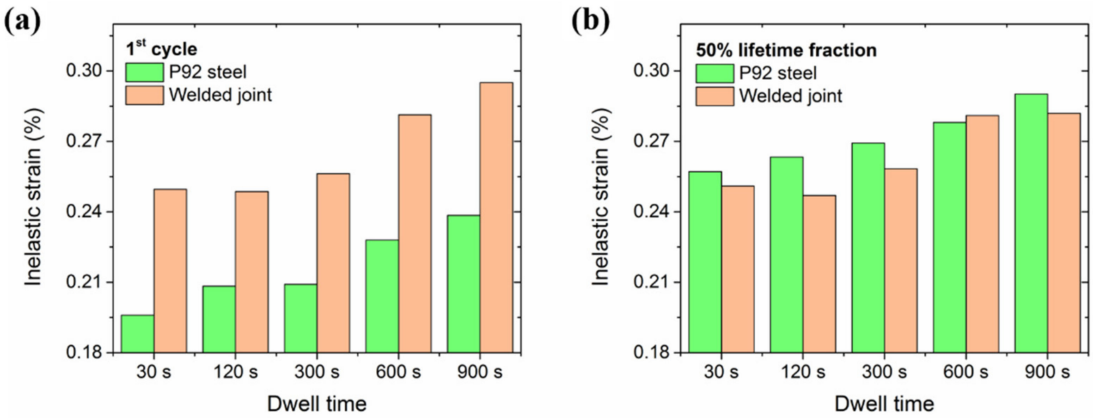

Figure 7. Variations in measured inelastic strain for welded and BM specimens with different holding times at (**a**) the 1st cycle and (**b**) 50% of the lifetime fraction.

3.2. Stress Relaxation Behavior

It is well known that stress relaxation can occur in the holding period during the strain-controlled CF test [9–12]. The typical stress relaxation behavior of the welded specimens during the tensile holding period (300 s) is shown in Figure 8. The magnitude of relaxed

stress is directly related to the amount of accumulated creep deformation, contributing to the variation in the inelastic strains [19,20]. To describe the stress relaxation behavior under different holding periods, the stress relaxation range σ_{rel} and stress level σ_{th} at the end of holding period were defined, as shown in Figure 8. Figure 9a compares the development of the stress relaxation range σ_{rel} for welded and BM specimens, which were subjected to different holding times. The data of five cycles around 50% of the cyclic life were used to describe the stress relaxation range. It can be seen that the stress relaxation range increased as the holding time increased for both kinds of specimens. The stress relaxation ranges of welded specimens were similar to those of the BM specimens, except for the one with a holding time of 30 s. As the number of cycles increased to 50% of the lifetime fraction, the stress relaxation range gradually increased for both kinds of specimens. Compared with the welded specimens, the degeneration of stress relaxation for the BM specimens was more remarkable.

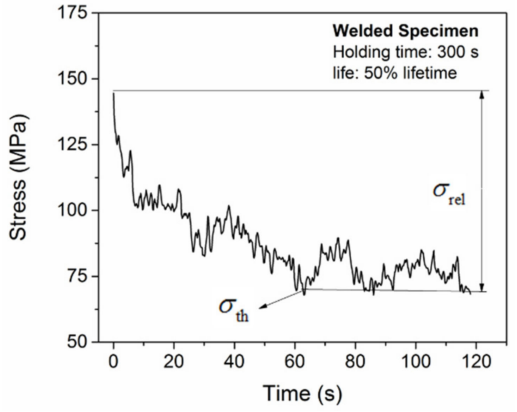

Figure 8. Typical stress relaxation curves of the welded specimen with a holding time of 300 s at 50% of the lifetime fraction.

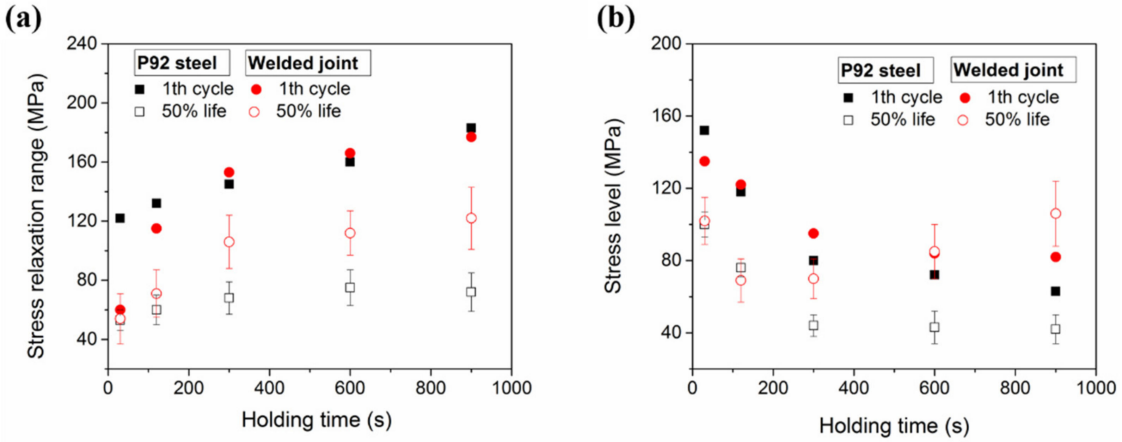

Figure 9. (**a**) Stress relaxation range and (**b**) stress level of all the welded and BM specimens at the 1st cycle and 50% of the lifetime fraction.

Figure 9b shows that the σ_{th} (stress level at end of holding period) for all of the welded and BM specimens at the first cycle and 50% of the lifetime fraction. Similarly, the data of five cycles around 50% of the cyclic life were used to describe the stress level. The σ_{th} for the BM specimens were observed to decrease with increasing holding times, and they gradually became saturated at approximately 70 MPa, as shown in Figure 9b. As for the welded specimens, the similar trend of σ_{th} was also obtained at the first cycle. However, after a rapid reduction in σ_{th} for the specimens with short holding times, they were slightly enhanced for specimens with long holding times (600 and 900 s). Furthermore, the values of

σ_{th} for the welded specimens were higher than the values for the BM specimens, especially for the specimens with long holding times. It has been speculated that the inhomogeneity in the welded specimen could be responsible for the higher values of σ_{th}. Since the CF experiments were all strain-controlled, the FGHAZ and BM regions (lower hardness) could have promoted more remarkable local deformation during tensile or compressive loading. During the holding period, these two regions firstly began to undergo stress relaxation due to their relatively lower hardness. As outlined above, an excessive Mo content could reduce the ductility and stability of the WM region, leading to a more remarkable reduction in the hardness of the WM region during the CF tests. Therefore, the WM region (higher hardness) would be continuously producing inelastic strain to compensate for the local stress during the holding period. This process also results in a more remarkable reduction in the hardness of the WM region, which was observed in the previous study [10]. Therefore, the values of σ_{th} for the welded specimens are higher than those of the BM specimens, which have homogeneous material properties.

3.3. Fracture Mechanism

To demonstrate the fracture mechanism of CF-failed specimens, Figure 10 displays the fractographies of the welded and BM specimens with short and long holding times, respectively. Fatigue striations were observed in all specimens, as shown in Figure 10a–d. Compared with the welded specimens, more pronounced fatigue striations were produced in the fracture surface of the BM specimens, indicating that the more severe fatigue damage was induced in the BM specimens during the main-fatigue-crack propagation. This deduction can be proved by the shorter cyclic lifetimes at the third stage (high propagation rate) for the BM specimens (Figure 5a).

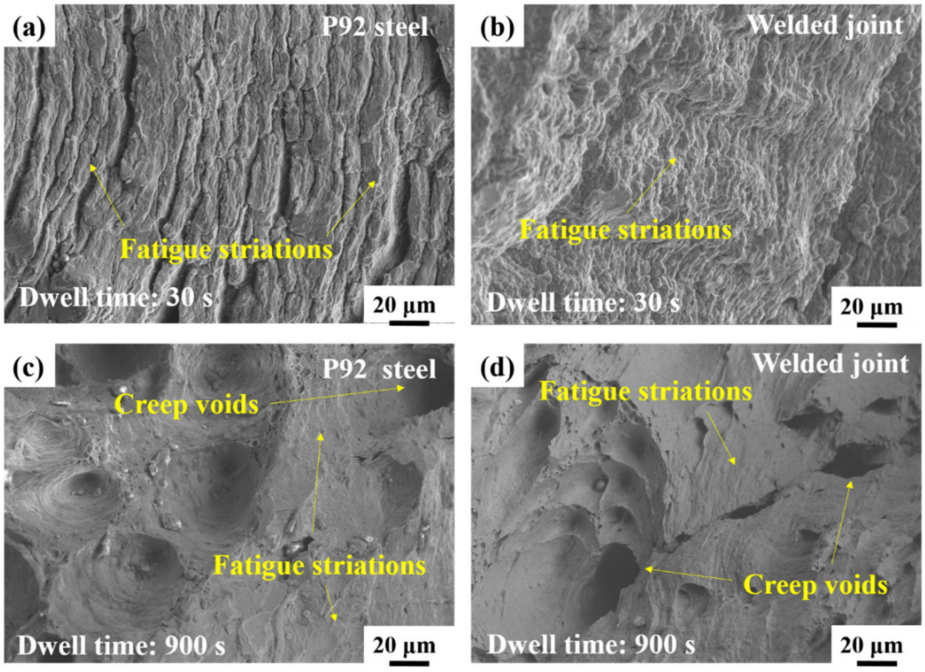

Figure 10. Fractographies of the BM specimens under creep-fatigue loading with (**a**); short and (**c**) long holding times. Fractographies of the welded specimens under creep-fatigue loading with (**b**) short and (**d**) long holding times.

Figure 10c,d show the fractographic images of the BM and welded specimens under creep-fatigue loading with holding times. The creep voids and dimples were clearly seen in the welded specimens with long holding times, as well as the BM specimens. It should be noted that more creep voids were observed in the fracture surfaces of the welded specimens. It is widely accepted that the creep voids are formed at the grain boundary with

high stress concentration during the holding periods [5,6]. The higher values of σ_{th} could result in higher stress levels in the welded specimens during the holding period (900 s), so as to produce more severe creep damage at the grain boundaries. It should be noted that although the stress levels of the welded specimens with holding times of 120, 300 and 600 s were higher than the BM specimens, their stress levels were still less than the threshold value of creep stress (90 MPa [20]). As the stress was lower than this threshold value, the effect of creep deformation on stress relaxation gradually diminished [20]. Thus, the cyclic life of those welded specimens were slightly higher than the BM specimens. However, the stress level of the welded specimen with a holding time of 900 s was 110 MPa, which is higher than the threshold value of creep stress (90 MPa [20]). The more severe creep damage inside the welded specimens with a holding time of 900 s can significantly reduce their cyclic life (548), which is shorter than the cyclic life (948) of the BM specimens. The observation of the fracture surface also proves that the fracture mechanisms of both kinds of specimens shifted from fatigue-dominated to creep-fatigue-interactive damage with increasing holding time. Since numerous creep voids were formed inside the P92 steel and welded joint, the period of the main-crack propagation was reduced, which led to the absence of a third cyclic softening period. Therefore, the fracture mechanism could be deduced to have shifted from fatigue-dominated damage to creep-fatigue interaction with increasing holding time (Figures 5 and 10).

4. Conclusions

This paper focuses on the fracture mechanism of Chinese P92 steel welded joints under creep-fatigue loading. The strain-controlled CF experiments with holding times of 30, 120, 300, 600 and 900 s were performed on welded specimens at 923 K, as well as base-metal (BM) specimens. The cyclic softening, inelastic strain amplitudes and stress relaxation behaviors were compared between welded and BM specimens. The following conclusions can be drawn:

1. From the results, the failure stage of welded specimens occupied 45% of the lifetime fraction, while it only took up 20% of the lifetime fraction in BM specimens with short holding times (30 and 120 s). Furthermore, only two softening stages were observed for both kinds of CF specimens with long holding times (300, 600 and 900 s for welded specimens; 600 and 900 s for base-metal specimens).
2. Compared with the welded specimens, the degeneration of stress relaxation for the BM specimens were more remarkable. The stress levels of the welded specimens were gradually larger than those of the BM specimens. It has been speculated that the inhomogeneity in the welded specimens could be responsible for the different stress relaxation behaviors.
3. Based on the observation of the fracture surfaces, the fracture mechanism shifted from fatigue-dominated damage to creep-fatigue interaction with increasing holding periods.

Author Contributions: Conceptualization, Y.L. and Y.S.; investigation, Y.S.; data curation, P.L.; writing—original draft preparation, Y.L.; writing—review and editing, Y.L. and T.J. All authors have read and agreed to the published version of the manuscript.

Funding: The research work was supported by the Key Technologies Program of Zhejing Province (No. 2019YFC03112) and the Fundamental Research Funds for the Provincial Universities of Zhejiang (RF-A2020010) and National Natural Science Foundation of China (52075490).

Institutional Review Board Statement: Not applicable.

Informed Consent Statement: Not applicable.

Data Availability Statement: The datasets supporting the conclusions of this article are included within the article.

Conflicts of Interest: The authors declare no conflict of interest.

References

1. Chang, L.; Li, X.; Wen, J.; Zhou, B.; He, X.; Zhang, G.; Xue, F.; Zhao, Y.; Zhou, C. Thermal-mechanical fatigue behaviour and life prediction of P92 steel, including average temperature and dwell effects. *J. Mater. Res. Technol.* **2020**, *9*, 819–837. [CrossRef]
2. Zhang, X.C.; Tu, S.T.; Xuan, F.Z. Creep-fatigue endurance of 304 stainless steels. *Theor. Appl. Fractue Mech.* **2014**, *71*, 51–66. [CrossRef]
3. Wang, X.; Zhang, W.; Zhang, T.; Gong, J.; Abdel Wahab, M. A new empirical life prediction model for 9–12% Cr steels under low cycle fatigue and creep fatigue interaction loadings. *Metals* **2019**, *9*, 183. [CrossRef]
4. Kannadasan, G.; Kumar, R.; Sahu, J.; Ray, P.; Ghosh, R. Designing P92 grade martensitic steel header pipes against creep–fatigue interaction loading condition: Damage micromechanisms. *Mater. Des.* **2015**, *86*, 411–420.
5. Zhang, W.; Zhang, T.; Wang, X.; Chen, H.; Gong, J. Remaining creep properties and fracture behavior of P92 steel welded joint under prior low cycle fatigue loading. *J. Mater. Res. Technol.* **2020**, *9*, 7887–7899. [CrossRef]
6. Zhang, W.; Wang, X.; Chen, H.; Zhang, T.; Gong, J. Evaluation of the effect of various prior creep-fatigue interaction damages on subsequent tensile and creep properties of 9%Cr steel. *Int. J. Fatigue* **2010**, *125*, 440–453. [CrossRef]
7. Veerababu, J.; Goyal, S.; Nagesha, A. Studies on creep-fatigue interaction behavior of Grade 92 steel and its weld joints. *Int. J. Fatigue* **2021**, *149*, 106307. [CrossRef]
8. Pandey, C.; Mahapatra, M.M.; Kumar, P.; Vidyrathy, R.S.; Srivastava, A. Microstructure-based assessment of creep rupture behaviour of cast-forged P91 steel. *Mater. Sci. Eng. A* **2017**, *695*, 291–301. [CrossRef]
9. Song, Y.; Qin, F.; Chen, J.; Pan, Z.; Huang, X.; Ding, Z.; Gao, Z.; Zhang, T.; Ma, Y. On the microstructural evolution and room-temperature creep behavior of 9%Cr steel weld joint under prior creep-fatigue interaction. *Fatigue Fract. Eng. Mater. Struct.* **2021**, *44*, 444–460. [CrossRef]
10. Song, Y.; Pan, Z.; Chen, J.; Qin, F.; Gao, Z.; Zhang, T.; Ma, Y. The effects of prior creep-fatigue interaction on the strain rate sensitivity of a P92 steel weld joint. *J. Mater. Sci.* **2021**, *56*, 7111–7128. [CrossRef]
11. Song, Y.; Ma, Y.; Chen, H.; He, Z.; Chen, H.; Zhang, T.; Gao, Z. The effects of tensile and compressive dwells on creep-fatigue behavior and fracture mechanism in welded joint of P92 steel. *Mater. Sci. Eng. A* **2021**, *813*, 141129. [CrossRef]
12. Song, Y.; Dai, Y.; Gao, Z.; Huang, H.; Chen, H.; Ma, Y. Probing strain rate effect on the creep–fatigue fracture mechanism of 9%Cr steel-welded joint via nanoindentation characterization. *Fatigue Fract. Eng. Mater. Struct.* **2021**. [CrossRef]
13. Gao, Z.; Song, Y.; Pan, Z.; Chen, J.; Ma, Y. Nanoindentation investigation on the creep behavior of P92 steel weld joint after creep-fatigue loading. *Int. J. Fatigue* **2020**, *134*, 105506. [CrossRef]
14. Brinkman, C.R.; Alexander, D.J.; Maziasz, P.J. Modified 9Cr–1Mo steel for advanced steam generator applications. In Proceedings of the ASME/IEEE Power Generation Conference, Boston, MA, USA, 21–25 October 1990; pp. 1–8.
15. Matsui, M.; Tabuchi, M.; Watanabe, T.; Kubo, K.; Kinugawa, J.; Abe, F. Degradation of creep strength in welded joint of 9% Cr steel. *ISIJ Internat.* **2001**, *41*, 126–130. [CrossRef]
16. Albert, S.K.; Matsui, M.; Watanabe, T.; Hongo, H.; Kubo, K.; Tabuchi, M. Variation in the type IV cracking behavior of a high Cr steel weld with post weld heat treatment. *Int. J. Press. Vessel. Pip.* **2003**, *80*, 405–413. [CrossRef]
17. Wu, X.J. *Deformation and Life Evolution in Crystalline Materials-the Integrated Creep-Fatigue Theory*; CRC Press: Boca Raton, FL, USA, 2019.
18. Fatemi, A.; Yang, L. Cumuative fatigue damage and life prediction theories: A survey of the state of the art for homogeneous materials. *Int. J. Fatigue* **1998**, *20*, 9–34. [CrossRef]
19. Wang, R.Z.; Zhang, X.C.; Tu, S.T.; Zhu, S.P.; Zhang, C.C. A modified strain energy density exhaustion model for creep-fatigue life prediction. *Int. J. Fatigue* **2016**, *90*, 12–22. [CrossRef]
20. Zhao, L.; Xu, L.; Han, Y.; Jing, H. Analysis on stress-strain behavior and life prediction of P92 steel under creep-fatigue interaction conditions. *Fatigue Fract. Eng. Mater. Struct.* **2020**, *43*, 2731–2743. [CrossRef]
21. ASME. *Boiler & Pressure Vessel Code Part II -2015*; ASME: Singapore, 2015.
22. Song, Y.X.; Ma, Y.; Pan, Z.X.; Li, Y.B.; Zhang, T.H.; Gao, Z.L. Nanoindentation characterization of creep-fatigue interaction on local creep behavior of the P92 steel welded joint. *Chin. J. Mech. Eng.* **2021**, accepted.
23. Wang, X.; Zhang, W.; Gong, J.; Jiang, Y. Experimental and numerical characterization of low cycle fatigue and creep fatigue behaviour of P92 steel welded joint. *Fatigue Fract. Eng. Mater. Struct.* **2018**, *41*, 611–624. [CrossRef]
24. Wan, R.; Sun, F.; Zhang, L.; Shan, A. Effect of Mo addition on strength of fire-resistant steel at elevated temperature. *J. Mater. Eng. Perform.* **2014**, *2*, 2780–2786. [CrossRef]